On the Spatial Resolution of GNSS Reflectometry

Maria Paola Clarizia, *Member, IEEE*, and Christopher S. Ruf, *Fellow, IEEE*

***Abstract*—A method for defining the spatial resolution of a Global Navigation Satellite System reflectometry delay–Doppler map (DDM) and of any derived geophysical product is proposed. An effective spatial resolution is derived as a function of measurement geometry and delay–Doppler (DD) interval, and as a more appropriate representation of resolution than the geometric resolution previously used in the literature. The definition more accurately accounts for variations in the scattered power across different pixels of the DDM and more accurately includes the power spreading effect caused by the Woodward ambiguity function. The dependence of the effective resolution on incidence angle, receiver altitude, and DD interval is analyzed and compared with the dependence of the geometric resolution with similar parameters.**

***Index Terms*—Delay–Doppler map (DDM), Global Navigation Satellite System reflectometry (GNSS-R), resolution.**

I. Introduction

GLOBAL navigation satellite system reflectometry (GNSS-R) is recognized as a promising remote sensing technique that fulfills the need for high spatial coverage, short temporal revisit time, and reduction in cost for satellite missions.

The most successful application of GNSS-R for ocean remote sensing so far is the retrieval of surface roughness and near-surface wind speed [1]–[5]. The typical algorithms used to estimate the wind and wave parameters in scatterometric GNSS-R can be divided into two categories: 1) approaches that exploit the delay–Doppler map (DDM) over a selected delay–Doppler (DD) window, centered around the specular point, to retrieve the geophysical parameters of interest, usually through the definition of an observable [3]–[5] or by fitting a model to the DDM [2]; and 2) approaches that perform a DDM deconvolution and a DD-to-space inversion to obtain an image of the normalized radar cross section [7] and, hence, of the wind speed or wave field over a given area. The first type of algorithm is more commonly used due to the difficulty in deconvolving the DDM and in resolving the space-to-DD ambiguity [1].

However, assigning a spatial resolution to the geophysical parameters estimated from a particular DD region presents challenges. One previous wind speed retrieval study assigned a spatial resolution to their wind product that is purely based on geometrical considerations [5]. Consideration on how to determine the spatial resolution is discussed in [6] without a specific mathematical definition.

Manuscript received November 30, 2015; revised March 3, 2016; accepted April 29, 2016. Date of publication June 2, 2016; date of current version July 20, 2016.

The authors are with the Department of Climate and Space Sciences and Engineering, University of Michigan, Ann Arbor, MI 48109-2143 USA.

Color versions of one or more of the figures in this paper are available online at http://ieeexplore.ieee.org.

Digital Object Identifier 10.1109/LGRS.2016.2565380

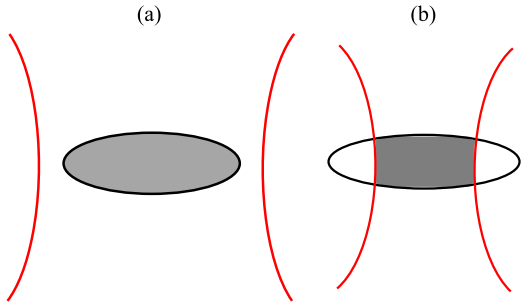

Fig. 1. (a) Geometric case 1: When the iso-Doppler lines at the minimum and maximum Doppler frequencies of the selected interval (red parabola) do not cross the iso-delay line (black ellipse) at the maximum delay of the selected interval. (b) Geometric case 2: When the iso-Doppler parabola crosses the iso-delay ellipse. In both cases, the geometric resolution is the square root of the gray area.

Here, a definition of effective spatial resolution is proposed, which expands on the geometric resolution (i.e., the area at the intersection of the maximum iso-delay and iso-Doppler lines of the DD window [5], [8]) by incorporating the effect of varying scattered power across the physical area and the spreading effect of the Woodward ambiguity function (WAF). For simplicity, we focus on GPS signals with the WAF illustrated in [9]. Our definition can be extended to other types of navigation signals with different WAFs. The effective spatial resolution is described as a function of geometry (i.e., receiver altitude and incidence angle) and a size of the DD interval, and can be used to assign a spatial resolution to any geophysical parameter retrieved from a DDM. This letter is organized as follows. Section II summarizes the definition of geometric resolution and presents a formal mathematical definition of the effective spatial resolution. Section III illustrates the dependence of effective spatial resolution on incidence angle (see Section III-A), receiver altitude (see Section III-B), and DD interval (see Section III-C), and compares the effective spatial resolution with geometric spatial resolution in all three cases. Section IV presents a compact polynomial approximation of the full formulation of the effective spatial resolution, and Section V summarizes the conclusions of this letter.

II. Definition of Spatial Resolution

The geometric spatial resolution corresponding to a given DD interval in GPS-reflectometry (GPS-R) has been defined in [5] as the square root of the spatial scattering area within the DD interval considered, i.e., the area at the intersection between the iso-delay ellipse at the maximum delay considered, and the two iso-Doppler parabolas at the minimum and maximum Doppler frequencies considered. Two possible configurations of iso-Delay ellipses and iso-Doppler lines are illustrated in Fig. 1, for a given geometry and DD interval.

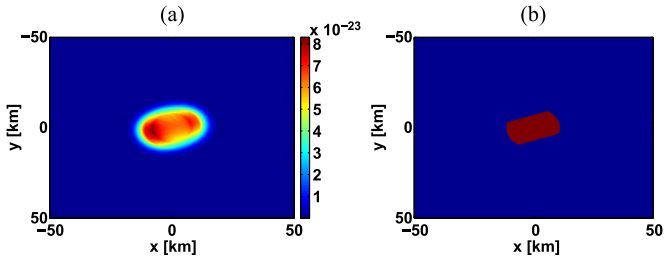

Fig. 2. (a) Weighting function and (b) physical scattering area for $h_0 = 500$ km, $\theta = 20°$, $\tau_L = 1$ chip, and $|f_M^D| = 2000$ Hz.

Hence, the geometric spatial resolution can be either determined by the iso-delay ellipse only when the iso-Doppler lines fall outside the area delimited by the ellipse (see case 1 in Fig. 2) or by the actual intersection of iso-delay ellipse and iso-Doppler lines (see case 2 in Fig. 2). This definition of spatial resolution relies purely on geometrical considerations and does not take into account: 1) the variations in the received power across the different points within the DD window boundaries; and 2) the "residual" scattered power from points immediately outside the DD window boundaries, as a result of the spreading caused by the WAF. An alternate "effective" spatial resolution is proposed, whose definition takes into account both the aforementioned effects. The total received power P_{tot} over a given DD interval can be expressed as

$$P_{\text{tot}} = \sum_{l=1}^{L} \sum_{m=-M}^{M} P_{\text{DDM}}\left(h_0, \theta, \tau_l, f_m^D\right) \tag{1}$$

where P_{DDM} is the received power in a single pixel of the DDM; h_0 is the receiver altitude; θ is the incidence angle (see Fig. 7 in the Appendix); τ_l and f_m^D are the delay and Doppler coordinates, respectively; and the summation extends over the L discrete delay pixels and $2M+1$ discrete Doppler pixels that form the selected DD interval. The individual DDM pixels can be expressed as

$$P_{\text{DDM}}\left(h_0, \theta, \tau_l, f_m^D\right) = \int_S \sigma_0(x, y, h_0, \theta) W\left(x, y, h_0, \theta, \tau_l, f_m^D\right) dxdy \tag{2}$$

where the integral is over the portion of the Earth surface S forming the glistening zone, and $W(\ldots)$ is a weighting function comprised of all the other terms in the bistatic GPS scattering equation [9]. The weighting function can be written as

$$W\left(x, y, h_0, \theta, \tau_l, f_m^D\right) = K \frac{G_R}{R_T^2 R_R^2} \text{WAF}^2\left[t, \tau_l, f^D, f_m^D\right] \tag{3}$$

where

a) $K = \lambda^2 P_T G_T / (4\pi)^3$ with λ as the GPS wavelength and G_T and P_T being, respectively, the transmit antenna gain and power;
b) $t = t(x, y, \theta, h_0)$ and $f^D = f^D(x, y, \theta, h_0)$ are the delay and Doppler frequency coordinates corresponding to the space coordinates (x, y);
c) $G_R = G_R(x, y, \theta, h_0)$ is the receive antenna gain;
d) $R_T = R_T(x, y, \theta, h_0)$ and $R_R = R_R(x, y, \theta, h_0)$ are the distances from the scattering point on the glistening zone at (x, y, z) to, respectively, the transmitter and receiver;
e) and WAF is the Woodward ambiguity function, expressed in [9].

Our definition for effective spatial resolution is adapted from a definition of effective bandwidth commonly used in the filter theory [10]. We consider the summation of the weighting function over the entire DD window, i.e.,

$$I_W = \sum_{l=1}^{L} \sum_{m=-M}^{M} \int_S W\left(x, y, h_0, \theta, \tau_l, f_m^D\right) dxdy \tag{4}$$

and we consider an equivalent quantity given by the following product:

$$I'_W = R_{\text{eff}}^2\left(h_0, \theta, \tau_L, f_M^D\right) \cdot W_{\text{avg}}\left(h_0, \theta, \tau_L, f_M^D\right) \tag{5}$$

where the average weighting function is given by

$$W_{\text{avg}}\left(h_0, \theta, \tau_L, f_M^D\right) = \frac{\sum_{l=1}^{L} \sum_{m=-M}^{M} \int_S W(x,y,h_0,\theta,\tau_l,f_m^D) \Pi\left(\frac{\tau_l - \tau_L/2}{\tau_L}\right) \cdot \Pi\left(\frac{f_m^D}{2f_M^D}\right) dxdy}{\sum_{l=1}^{L} \sum_{m=-M}^{M} \int_S \Pi\left(\frac{\tau_l - \tau_L/2}{\tau_L}\right) \cdot \Pi\left(\frac{f_m^D}{2f_M^D}\right) dxdy} \tag{6}$$

and the functions Π are rectangular functions.

We impose $I_W = I'_W$ and define the effective spatial resolution as

$$R_{\text{eff}}\left(h_0, \theta, \tau_L, f_M^D\right) = \sqrt{\frac{\sum_{l=1}^{L} \sum_{m=-M}^{M} \int_S W\left(x, y, h_0, \theta, \tau_l, f_m^D\right) dxdy}{W_{\text{avg}}\left(h_0, \theta, \tau_L, f_M^D\right)}}. \tag{7}$$

For brevity, we omit the dependence of R_{eff} on $(h_0, \theta, \tau_L, f_M^D)$. By combining (6) and (7), we rewrite R_{eff} as (8), shown at the bottom of the next page, where R_{GEO} is the geometric resolution, given by

$$R_{\text{geo}}\left(h_0, \theta, \tau_L, f_M^D\right) = \sqrt{\sum_{l=1}^{L} \sum_{m=-M}^{M} \int_S \Pi\left(\frac{\tau_l - \tau_L/2}{\tau_L}\right) \cdot \Pi\left(\frac{f_m^D}{2f_M^D}\right) dxdy}. \tag{9}$$

The expression for R_{eff} can be made more explicit by writing each term in $W(\ldots)$ as a function of the incidence angle θ, the receiver altitude h_0, and the DD region considered, delimited by 0 and τ_L in delays, and by $-f_M^D$ to f_M^D in Doppler frequency, as illustrated in the Appendix.

The determination of $R_{\text{eff}}(\ldots)$ is performed by defining the geometry and DD parameters θ, h_0, and τ_L, and by calculating

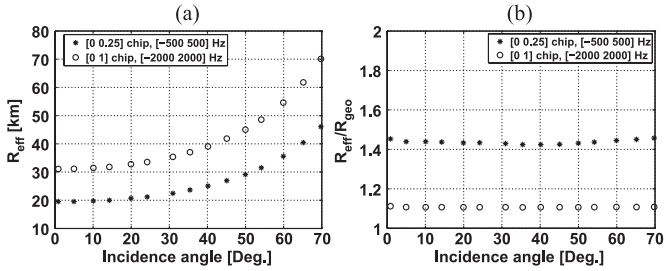

Fig. 3. (a) Effective resolution and (b) ratio between effective and geometric resolutions as a function of the incidence angle, for $h_0 = 500$ km, and two DD intervals of, respectively, (black stars) 0–0.25 chips/−500–500 Hz and (white circles) 0–1 chips/−2000–2000 Hz.

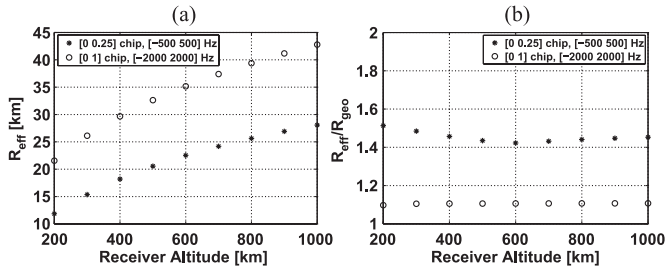

Fig. 4. (a) Effective resolution and (b) ratio between effective and geometric resolutions as a function of the receiver altitude, for $\theta = 20^\circ$ and the same DD intervals in Fig. 3.

the effective spatial resolution using (3), (8), and (9). Note that the effective spatial resolution should also ideally depend on the azimuth angle (i.e., the angle formed by the receiver velocity vector and the x-axis of the specular frame) through the orientation of the receiver velocity vector. However, this dependence is, in practice, small compared with the dependence on incidence angle and thus neglected here. Fig. 2 shows an example of the weighting function and physical area for a specified receiver altitude, incidence angle, and DD interval. A spherical Earth approximation has been used to determine the z-coordinate z_i of the surface points, and the receiver antenna gain $G_R(\ldots)$ has been calculated using the Cyclone Global Navigation Satellite System (CYGNSS) 2-D antenna pattern (see Appendix).

Fig. 2 highlights how different weights are assigned to the locations contributing to the scattered power and how the actual area covered by the weighting function is larger than the geometric area. However, the two areas become closer for increasing the DD interval, as described in Section III.

III. Dependence of R_{eff} on Geometry and DD Parameters

Variations in the effective spatial resolution as a function of the incidence angle, the receiver altitude, and the DD interval are considered, and the dependencies are compared with those of the geometric resolution.

A. Dependence on the Incidence Angle

The effective spatial resolution is shown as a function of the incidence angle in Fig. 3(a) for two different DD intervals. Fig. 3(b) illustrates the dependence of the ratio between effective and geometric resolutions on incidence angle, for the same DD intervals as in Fig. 3(a). Fig. 3(a) demonstrates that the effective spatial resolution increases with increasing incidence angle, similarly as the geometric resolution [5]. The similarity of their dependence on incidence angle is confirmed by Fig. 3(b), where the ratio exhibits little variation with respect to incidence angle for both the DD intervals considered.

B. Dependence on Attitude

The effective spatial resolution is also considered for varying receiver altitudes, assuming a constant incidence angle and the same DD intervals as the aforementioned. A plot of R_{eff} as a function of altitude is shown in Fig. 4(a). The effective resolution increases with altitude, as a result of the stretching of the iso-delay and iso-Doppler lines, i.e., the same DD interval covers a larger area. The geometric resolution is characterized by the same type of increase, and no significant difference is noted between their dependence on altitude, as shown in Fig. 4(b).

C. Dependence on DD Intervals

The effective resolution is considered at a fixed geometry (20° incidence angle, receiver altitude of 500 km) and for different DD intervals. The delay interval always starts at the zero chip delay (i.e., delay relative to the specular point) and its upper bound varies from 0.25–4 chips, with a step size of 0.25 chips. The Doppler interval varies from $[-500 \;\; 500]$ to $[-4000 \;\; 4000]$ Hz, with a step size of ± 500 Hz for the lower and upper Doppler bounds. Fig. 5(a) and (b) shows the 2-D map of effective resolution and ratio between effective and geometric resolutions as a function of the delay and Doppler intervals.

Fig. 5(a) and (b) shows that the geometric resolution is lower than the effective resolution at the small DD interval, whereas they tend to become closer for increasing DD intervals, which is confirmed by the tendency of their ratio to become close to unity in Fig. 5(b). The stronger differences for the small delay and Doppler intervals occur because the "additional area," introduced by the weighting function at the edges of the geometric area, is usually a larger proportion of the geometric area itself when this area is small and reduces as the geometric

$$R_{\text{eff}} = \sqrt{\frac{\sum_{l=1}^{L}\sum_{m=-M}^{M}\int_S W\left(x,y,h_0,\theta,\tau_l,f_m^D\right)dxdy}{\sum_{l=1}^{L}\sum_{m=-M}^{M}\int_S W\left(x,y,h_0,\theta,\tau_l,f_m^D\right)\Pi\left(\frac{\tau_l-\tau_L/2}{\tau_L}\right)\cdot\Pi\left(\frac{f_m^D}{2f_M^D}\right)dxdy}}\,R_{\text{geo}} \tag{8}$$

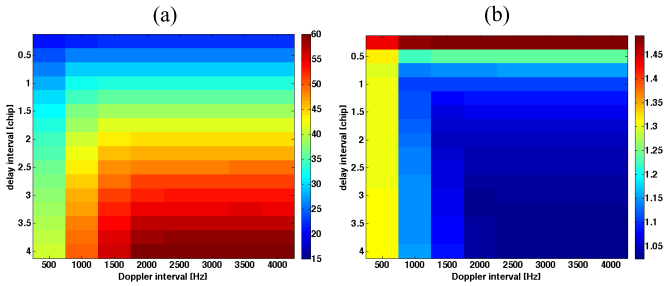

Fig. 5. (a) Effective resolution in kilometers and (b) ratio between effective and geometric resolutions as a function of DD interval.

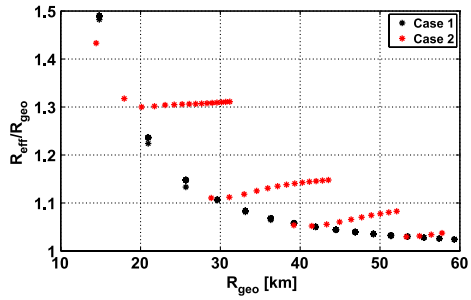

Fig. 6. Ratio of effective to geometric resolution versus geometric resolution for $h_0 = 500$ km, $\theta = 20°$, and all the different DD intervals shown in Fig. 5. Cases 1 and 2 refer to the configuration of iso-delay and iso-Doppler lines illustrated in Fig. 1.

area gets larger. This is, however, strictly true only when the iso-Doppler lines at the minimum and maximum Doppler of the interval considered are outside the iso-delay ellipse at the maximum delay, i.e., when case 1 of Fig. 1 occurs. Variations in the geometric and effective areas in the two cases highlighted in Fig. 1 are illustrated in Fig. 6, where the ratio of effective resolution to geometric resolution is plotted versus the geometric resolution and color coded for cases 1 and 2.

Fig. 6 shows a monotonic decrease in the ratio of effective resolution to geometric resolution with increasing geometric resolution for case 1, with the ratio converging to unity for large areas. This happens when the resolution is determined only by the size of the iso-delay ellipse at the maximum delay, for which an elliptical annulus is introduced by the weighting function as an additional scattering area, and the width of this annulus decreases with increasing delay interval, due to the iso-delay ellipses becoming closer to each other [1]. The relationship is more complicated in case 2, when the iso-Doppler lines cut across the iso-Delay ellipse. In this case, the additional area introduced by the weighting function is a subset of the annulus, plus some additional area at the edges of the iso-Doppler segments cutting through the iso-Delay ellipse. Variations in this area with increasing DD interval is not monotonic and depends on the particular DD interval considered, as shown in the behavior of the red points in Fig. 6.

IV. Polynomial Formulation of Effective Spatial Resolution

The effective spatial resolution is a fairly complex function of four parameters, and as such, its numerical implementation can be lengthy and cumbersome. However, the dependence of the effective spatial resolution on the DD parameters τ_L and f_M^D is found to be relatively independent of the geometric parameters θ and h_0. This separability allows for an approximation of the effective spatial resolution to be formulated as the product of two functions as follows:

$$R_{\text{eff}}\left(h_0,\theta,\tau_L,f_M^D\right) = R_c \cdot_{\text{eff}} f(h_0,\theta)\cdot g\left(\tau_L,f_M^D\right)$$
$$R_c = \frac{1}{g\left(\tau_L = 0.25\text{chip}, f_M^D = 500\text{ Hz}\right)}. \quad (10)$$

The two functions $f(h_0,\theta)$ and $g(\tau_L, f_M^D)$ can be well approximated by polynomial functions of the fourth degree. The resulting equation and coefficients obtained by a least-squares fit are given in Table I. They have been obtained assuming the CYGNSS receiver antenna pattern, and they are strictly valid for delay ranges smaller than 10 chips. The fourth-degree best-fit polynomial functions produce an overall rms error of 0.08 km in case 1 and 0.57 km in case 2.

Equation (10) is a useful tool for a quick estimation of the effective spatial resolution, but it represents an approximation and as such produces an error. The error between the true and approximate values of the effective spatial resolution has been calculated as a percentage of the true value, for a variety of geometries and receiver altitudes, and for the two DD pairs with the values of, respectively, $[0\ \ 0.75]$ chip/$[-1000\ \ 1000]$ Hz, and $[0\ \ 1.5]$ chip/$[-3000\ \ 3000]$ Hz. This error can be as low as $\sim$0.5% for the smaller DD interval and the lowest altitude case analyzed (200 km), and increases up to $\sim$12% for the larger DD interval and the higher altitudes because the true effective resolution is itself larger in these cases, i.e.,

$$P(x,y) = a_1 + a_2x + a_3y + a_4x^2 + a_5xy + a_6y^2 + \cdots a_7x^3 + \cdots a_8x^2y + a_9xy^2 + a_{10}y^3 + a_{11}x^4 + a_{12}x^3y + a_{13}x^2y^2 + a_{14}xy^3 + a_{15}y^4.$$

TABLE I
Coefficients for the Polynomial Fit of the Fourth Degree of $f(h_0,\theta)$ and $g(\tau_L, f_M^D)$. The Variables x and y in the Polynomial Equation at the Top of the Table Represent f_m^D and τ_l in the Case of $g()$, and h_0 and θ in the Case of $f()$

Polynomial Coefficients	$f(h_0,\theta)$	$g(\tau_L, f_M^D)$
a_1	1.8637	12.3384
a_2	5.9877*10^{-5}	0.0109
a_3	-0.1057	11.4361
a_4	-7.4064*10^{-11}	-5.2219*10^{-6}
a_5	2.9795*10^{-7}	0.0038
a_6	0.0058	-2.5841
a_7	6.0589*10^{-17}	8.9722*10^{-10}
a_8	-5.9001*10^{-13}	-7.5572*10^{-7}
a_9	5.9450*10^{-9}	2.7078*10^{-5}
a_{10}	-1.4150*10^{-4}	0.2628
a_{11}	-2.1499*10^{-23}	-5.0566*10^{-14}
a_{12}	3.3281*10^{-19}	4.4403*10^{-11}
a_{13}	-2.8274*10^{-15}	2.1525*10^{-9}
a_{14}	-1.0504*10^{-11}	-2.7769*10^{-6}
a_{15}	1.7546*10^{-6}	-0.0108

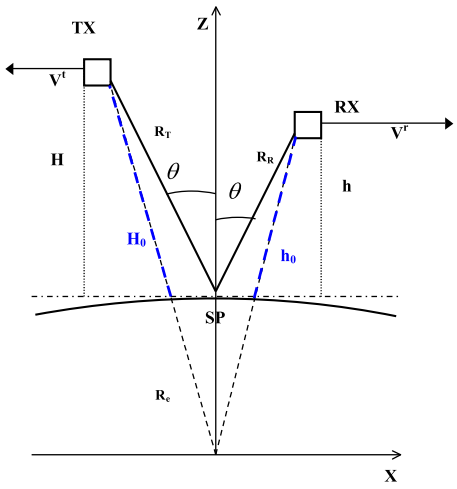

Fig. 7. Geometry and specular frame coordinate system. R_e is the Earth radius.

V. Conclusion

In this letter, we have presented a new definition of spatial resolution for DDM, called effective spatial resolution, following an approach similar to the definition of effective bandwidth that is typically used in the filter theory. An increase in the effective spatial resolution is observed for increasing incidence angle, receiver altitude, and DD window. The effective resolution is also compared with the geometric resolution, and the two exhibit the same general behavior with respect to changing measurement geometry and DD interval. The ratio between effective and geometric resolutions decreases with increasing geometric resolution, with the ratio tending toward unity at high ($>$ 60 km) geometric resolution and for large DD intervals, in particular when the iso-Doppler lines at the minimum and maximum Doppler frequency of the selected interval fall outside the iso-delay ellipse at the maximum delay. A concise polynomial approximation for the effective spatial resolution is also derived. It can be used as a convenient means for determining the effective spatial resolution. The effective spatial resolution represents a more rigorous expression for the surface scattering area that contributes to the measurements in a DDM and in any geophysical product obtained from it.

Appendix

Here, explicit expressions for the terms in the weighting function $W(\ldots)$ in (3) are given. We assume that the transmitter, receiver, and specular point coordinates are expressed in a specular point frame, as illustrated in Fig. 7.

The transmitter has coordinates $\boldsymbol{P}^t = [-H\tan(\theta), 0, H + R_e]$, and receiver $\boldsymbol{P}^r = [h\tan(\theta), 0, h + R_e]$, where H and h are related to the transmitter and receiver altitudes H_0 and h_0 by

$$H = \frac{-R_e + \sqrt{R_e^2 + H_0^2 + 2H_0R_e + H_0^2\tan^2(\theta) + 2H_0R_e\tan^2(\theta)}}{1+\tan^2(\theta)}$$
$$h = \frac{-R_e + \sqrt{R_e^2 + h_0^2 + 2h_0R_e + h_0^2\tan^2(\theta) + 2h_0R_e\tan^2(\theta)}}{1+\tan^2(\theta)}. \tag{A1}$$

The delay and Doppler shifts t_i and f_i associated with a point on the surface $\boldsymbol{P}_i = [x_i, y_i, z_i]$ can be written as

$$t_i = \frac{1}{c}\left[R_T(x_i, y_i) + R_R(x_i, y_i)\right]$$
$$f_i = L_1\left[-\boldsymbol{V}_t(\boldsymbol{P}^t - \boldsymbol{P}_i)/R_T - \boldsymbol{V}_r(\boldsymbol{P}^r - \boldsymbol{P}_i)/R_R\right]/c \tag{A2}$$

where L_1 is the GPS frequency; c is the speed of light, R_T and R_R are the ranges from transmitter/receiver to the point $\boldsymbol{P}_i$, and $\boldsymbol{V}_t = [V_t^x\ V_t^y\ V_t^z]$ and $\boldsymbol{V}_r = [V_r^x\ V_r^y\ V_r^z]$ are, respectively, the transmitter and receiver velocity vectors in the specular frame. The receiver antenna gain $G_R(x_i, y_i)$ is a function of elevation angle ω_i and azimuth angle φ_i of the point $\boldsymbol{P}_i$ in the satellite orbit frame; hence, we need to relate ω_i and φ_i to x_i and y_i. The elevation and azimuth angles in the orbit frame for $\boldsymbol{P}_i$ on the surface can be written as

$$\omega_i = \tan^{-1}\left(\frac{\left\|\vec{V}^r\right\|\delta_i}{\sqrt{\left\|\vec{N}_c\right\|^2\alpha_i^2 + \beta_i^2}}\right)$$
$$\varphi_i = \tan^{-1}\left(\frac{\beta_i}{\|\vec{N}_c\|\alpha_i}\right)$$
$$\alpha_i = V_x^r\left(x_i - h\tan(\theta)\right) + V_y^r y_i + V_z^r(z_i - h - R_e)$$
$$\beta_i = V_y^r(R_e + h)\left(x_i - h\tan(\theta)\right) + \cdots + y_i\left[-V_z^r h\tan(\theta) - V_x^r(R_e + h)\right] + V_y^r(z_i - h - R_e)h\tan(\theta)$$
$$\delta_i = h\tan(\theta)\left(x_i - h\tan(\theta)\right) + (z_i - h - R_e)(-h - R_e)$$
$$\|\vec{N}_c\| = \sqrt{h^2\tan^2(\theta) + (-h - R_e)^2}. \tag{A3}$$

References

[1] S. Gleason, S. Hodgart, S. Yiping, C. Gommenginger, S. Mackin, M. Adjrad, and M. Unwin, "Detection and processing of bistatically reflected GPS signals from low Earth orbit for the purpose of ocean remote sensing," *IEEE Trans. Geosci. Remote Sens.*, vol. 43 no. 6, 1229–124, Jun. 2005.

[2] O. Germain *et al.*, "The Eddy experiment: GNSS-R speculometry for directional sea-roughness retrieval from low altitude aircraft," *Geophys. Res. Lett.*, vol. 31, no. 21, Nov. 2004, Art. no. L12306.

[3] J. Marchan-Hernandez *et al.*, "Sea-state determination using GNSS-R data," *IEEE Geosci. Remote Sens. Lett.*, vol. 7, no. 4, 621–625, Oct. 2010.

[4] M. P. Clarizia, C. S. Ruf, P. Jales, and C. Gommenginger, "Spaceborne GNSS-R minimum variance wind speed estimator," *IEEE Trans. Geosci. Remote Sens.*, vol. 52, no. 11, pp.6829–6843, Nov. 2014, doi: 10.1109/TGRS.2014.2303831.

[5] M. P. Clarizia and C. S. Ruf, "Wind speed retrieval algorithm for the Cyclone Global Navigation Satellite System (CYGNSS) mission," *IEEE Trans. Geosci. Remote Sens.*, vol. 54, no. 8, pp. 4419–4432, Aug. 2016.

[6] V. U. Zavorotny, S. Gleason, E. Cardellach, and A. Camps, "Tutorial on Remote Sensing Using GNSS bistatic radar of opportunity," *IEEE Geosci. Remote Sens. Mag.*, vol. 2, no. 4, pp. 8–45, Dec. 2014, doi: 10.1109/MGRS.2014.2374220.

[7] E. Valencia *et al.*, "Ocean surface's scattering coefficient retrieval by Delay–Doppler Map inversion," *IEEE Geosci. Remote Sens. Lett.*, vol. 8. no. 4, 750–754, Jul. 2011.

[8] S. Gleason, C. Ruf, M. P. Clarizia, and A. O'Brien, "Calibration and unwrapping of the normalized scattering cross section for the cyclone global navigation satellite system," *IEEE Trans. Geosci. Remote Sens.*, vol. 54, no. 5, pp. 2495–2509, May 2016, doi: 10.1109/TGRS.2015.2502245.

[9] V. Zavorotny and A. Voronovich, "Scattering of GPS signals from the ocean with wind remote sensing applications," *IEEE Trans. Geosci. Remote Sens.*, vol. 38, no. 2, 951–964, Mar. 2000.

[10] D. E. Johnson, *Introduction to Filter Theory*. Englewood Cliffs, NJ, USA: Prentice-Hall, 1976.